buildings

MDPI

Article

Nano Engineered Paraffin-Based Phase Change Material for Building Thermal Management

John Paul [1], Mahendran Samykano [1,*], Adarsh Kumar Pandey [2,3,*], Kumaran Kadirgama [1,*] and Vineeth Veer Tyagi [4]

[1] Faculty of Mechanical & Automotive Engineering Technology, Universiti Malaysia Pahang, Pekan 26600, Pahang, Malaysia
[2] Research Centre for Nanomaterials and Energy Technology (RCNMET), School of Engineering & Technology, Sunway University, No. 5, Jalan Universiti, Bandar Sunway, Petaling Jaya 47500, Selangor Darul Ehsan, Malaysia
[3] Center for Transdisciplinary Research (CFTR), Saveetha Institute of Medical and Technical Sciences, Saveetha University, Chennai, India
[4] School of Energy Management, Shri Mata Vaishno Devi University, Katra 182320, (J&K), India
* Correspondence: mahendran@ump.edu.my (M.S.); adarshp@sunway.edu.my (A.K.P.); adarsh.889@gmail.com (K.K.)

Abstract: Thermal energy storage (TES) and harvesting is an effective technique for optimum building thermal management. Phase-change materials (PCMs) are commonly used for TES applications but are troubled by their degraded thermal conductivity. Recent research progress in latent heat energy storage using PCMs and nano additives provides a viable solution for solar TES. A series of hybrid nano-enhanced phase change materials (HNePCMs) were prepared via two-step synthesis. Hybrid graphene–silver nanofillers were dispersed in commercial paraffin (melting point 25 °C) under different dispersion rates (0.1%, 0.3%, 0.5%). Different characterization techniques, e.g., FESEM, FT-IR, UV-VIS, TGA, XRD, DSC, and Tempos, were used in material characterization. A maximum enhancement of 6.7% in latent heat and 5% in heat storage efficiency was noted for nanocomposites with 0.3 wt% of additives. The nanocomposite with 0.3 Wt% showed great potential in shielding UV rays and showed a reduction of 6.5% in bandgap energy. Furthermore, the thermal conductivity of samples was boosted by a maximum of 90% (from 0.2 W/mK-0.39 W/mK) with 0.3 wt% dispersion of graphene–silver nanofillers. The thermophysical characterization results establish that the synthesized paraffin/graphene–silver hybrid nanocomposites are well suited for building thermal management.

Keywords: phase change materials; nanocomposites; graphene: silver nanofillers; building thermal management

Citation: Paul, J.; Samykano, M.; Pandey, A.K.; Kadirgama, K.; Tyagi, V.V. Nano Engineered Paraffin-Based Phase Change Material for Building Thermal Management. *Buildings* **2023**, *13*, 900. https://doi.org/10.3390/buildings13040900

Academic Editor: Ahmed Senouci

Received: 2 February 2023
Revised: 3 March 2023
Accepted: 11 March 2023
Published: 29 March 2023

1. Introduction

In recent decades, a profound rise in sustainable and clean energy technologies arose due to rising global energy demand and environmental challenges [1]. The inconsistency of sustainable energy sources (wind, tidal, and solar energy) reinforces the importance of energy storage [2]. Under the Paris Agreement signed by all United Nations member states in 2015, all its member states are bound to attain a reduction in carbon dioxide (CO_2) emissions mainly by curtailing their fossil fuel usage to 20%. Moreover, the agreement also put forward 17 Sustainable development goals (SDGs). Goal seven among the 17 SDGs stresses providing green and affordable energy around the globe, which literally stresses embracing energy-efficient and renewable energy resources [3]. Approximately 40% of global energy use occurs in the building sector. The general change in living standards and the greater need for heating and cooling in cold and hot climates are the leading causes of rising energy usage [4]. Thermal energy remains an abundant energy source, which is substantially present in nature and is also available as a derivate of numerous energy

conversion processes. Thermal energy storage (TES) presents a possible technique to reuse ample heat energy and enhance energy efficiency. TES could be implemented to harvest, store, and even reuse energy as heat whenever needed. Furthermore, it might also provide a viable solution for the existing problem of unmatched energy supply and demand in time and space [5]. Latent heat energy storage (LHES) unveils a higher energy storage density. It also holds a sensitive operating temperature range [6]. Phase change materials (PCMs) were deployed for LHES due to their excellent thermal energy storage capabilities, which resemble a thermal battery [7]. Organic, inorganic, and eutectics are the three main classes of phase change materials. Paraffin wax (PW), an organic PCM, remains the most widely preferred PCM owing to its peculiar attributes: (a) superior heat of fusion, (b) corrosion-free nature, (c) thermal cycling stability, (d) tuneable melting point (20–100 °C), and (e) economic viability. The prominent hurdle in promoting the widespread usage of paraffin as a TES element is its degraded thermal conductivity. Degraded thermal conductivity offers comparatively improved interfacial thermal resistance (among the PCM and dispersed filler), which degrades the charging efficiency of the energy storage material during TES [8]. Installing PCM-enhanced wallboards within the building envelope is the most prevalent technique for building thermal management. Therefore, PCMs can enhance thermal inertia of lightweight structures, resulting in a substantial rise in thermal storage capacity. In order to obtain more significant yearly energy savings, cooling dominant climates demand PCMs with a melting point near 26 °C, whereas heating dominant climates need a melting point closer to 20 °C [9].

Dispersing highly conductive fillers with nano-size provides a viable solution to improving the degraded thermal conductive nature of the PCM matrix. The impact of dispersing thermally conductive nanostructured materials commonly utilized as thermal conductivity enhancers was comprehensively reviewed [10,11]. A meta-analysis of nanofillers was also conducted based on their dimension (0-D,1-D, 2-D, 3-D, and even hybrid materials). Authors also concluded that carbon-based nanomaterials exhibited a higher enrichment in thermal conductivity when compared with metallic/metal oxide nanoparticles [10]. Infusing nanosized carbon-based nanomaterials as fillers is a commonly adopted method to boost the thermal conductivity (λ value) of composites [12]. The chemical exfoliation of graphite flakes generates graphite nanoplatelets, multilayer graphene, and graphene, which possess a higher aspect ratio and ultrahigh intrinsic thermal conductivity ((λ value) > 2000 Wm^{-1} K^{-1}). The loading rate of nanofillers, interfacial thermal resistance, geometrical and dimensional aspects of the dispersants, including size, thickness, and the orientation of sheets, largely influences the enhancement in λ values [13]. The improvement in effective λ value is not pronounced when individual 2D materials are doped onto PCMs. This is primarily because of disorganized geometric contact and interfacial thermal resistance, which is normally elevated when the nanoparticles generate a disordered percolation network [14]. The dispersed fillers could also contribute to unstable λ value during phase transitions [15]. The dispersion of nano-fillers mainly alters the thermal conductivity of the base matrix and even other characteristics, including enthalpy, sub-cooling, phase transition temperature, phase transition duration, density, and viscosity [11]. The excellent thermal conductivity and chemical stability make silver (Ag) another suitable nano-sized dispersant for PCMs. PCM dispersed with mono nanofillers were comprehensively analyzed, and it was understood that the dispersion modifies the thermophysical properties of composites. Moreover, studies on PCMs (especially paraffin) infused with hybrid nanofillers are much fewer or even limited when compared with single nanofillers infused PCMs [10]. PCMs have been widely deployed for thermal management in buildings. The suitability of engineered phase change composites in the thermal management of buildings has been reviewed in detail [16].

George et al. [17] conducted a comparative analysis by dispersing both Polyaniline (PANI) and CuO in paraffin. The rise in thermal conductivity was around 46.7% and 63.5% for PANI and CuO, and the latent heat also logged an increment of 8.25 and 7.8% rise. Habib et al. [18] obtained a boost of 60.5% in thermal conductivity with SWCNT doped into

paraffin. Sheng et al. [19] used carbon fiber as a nano additive, and the thermal conductivity was boosted by 148%. The graphene dispersion in paraffin reported by Joseph et al. [20] provided an increment of 60.55 in thermal conductivity. Aslfattahi et al. [21] successfully doped MXene into the paraffin, and the composite registered an improvement of 11.6% in thermal conductivity. Table 1 briefly summarizes the thermophysical properties of recent research works on different paraffin-based nanocomposites. An in-depth literature review by Paul et al. [10,22] highlighted a lack of investigations into the synthesis and thermophysical characterization of low-temperature organic NePCMs used in ambient conditions. Hence, this proved to be an aspiration for researchers in developing low-temperature composite PCMs dispersed with hybrid nanofiller for building thermal management.

Table 1. Thermophysical properties of wax-based nanocomposites.

Nanocomposites	Change in Thermal Conductivity (W/mK)	Change in Enthalpy (J/g)	Nanocomposites	Ref.
Paraffin/Graphene	59.5% increment	12.4% decline	Paraffin/Graphene	[20]
Paraffin/CNT	39.0% increment	0.90% decline	Paraffin/CNT	[23]
Paraffin/PANI	46.7% increment	8.20% increment	Paraffin/PANI	[17]
Paraffin/CuO	63.5% increment	7.80% increment	Paraffin/CuO	[17]
Paraffin/Co-PANI	17.6%increment	8.06% decline	Paraffin/Co-PANI	[24]
Paraffin/Nanographene	741% increment	13.10% decline	Paraffin/Nanographene	[25]
Paraffin/GP: Ag	90% increment	6.70% increment	Paraffin/GP: Ag	PW

In summary, we demonstrate a method to achieve superior λ values with hybrid nano-enhanced phase change materials (HNePCM) formulated via two-step method for the thermal management of buildings and other ambient temperature applications. To the best of our knowledge, the synthesis of HNePCM loaded with 2-D graphene–silver nanofillers in low-temperature paraffin remains a novel work. A maximal enrichment of 90% in thermal conductivity was clocked for the 0.3% dispersion of nano additives. The synergistic effect of hybrid nanofillers, low interfacial thermal resistance, and reagglomeration contribute to an exceptional increment in λ. The λ value of HNePCMs could be tailored within a range of 0.2–0.4 W/mK with nanofiller loadings limited to 0.5 wt%. The composites displayed excellent photo-thermal absorption, latent heat (6.7%), thermal stability (5.7 °C), and reliability. The hybrid nanocomposites could shield UV radiation to a maximum of 100%. The present work provides insights into the exceptional enhancement in the λ value of composites by dispersing hybrid additives, which are currently restricted to PCM-based composites but could also be used to design scalable and higher power density thermal energy harvesting devices for building thermal management applications.

2. Experimental Section

2.1. Materials and Methods

Commercial grade paraffin wax (Plus ice A25 H), purchased from Plus Ice UK, was used as the TES material. Graphene–silver hybrid nanoparticles (with ratio 7:3) was procured from US Research Nanomaterials, Inc, and SDBS was procured from Sigma Aldrich. The entire chemicals used in the synthesis procedure were of analytical reagent grade.

2.2. Synthesis of Paraffin/Graphene: Silver Hybrid Nanocomposites

Two-step synthesis was adopted to synthesize the nanocomposite. The paraffin was heated to ensure a homogeneous liquid state. A calculated quantity of surfactant (SDBS) and liquid PCM mixture was subjected to probe sonication for 40 min. Graphene–silver hybrid nanoflakes were dispersed into the melted wax and further put to probe sonication for 40 min to ensure the homogenous mixing of dispersed additives. Figure 1 details the synthesis route of hybrid nanocomposites. The sonicated mixture was then allowed to cool down to ambient temperature. Figure 2 shows the images of pure and synthesized hybrid nanocomposites.

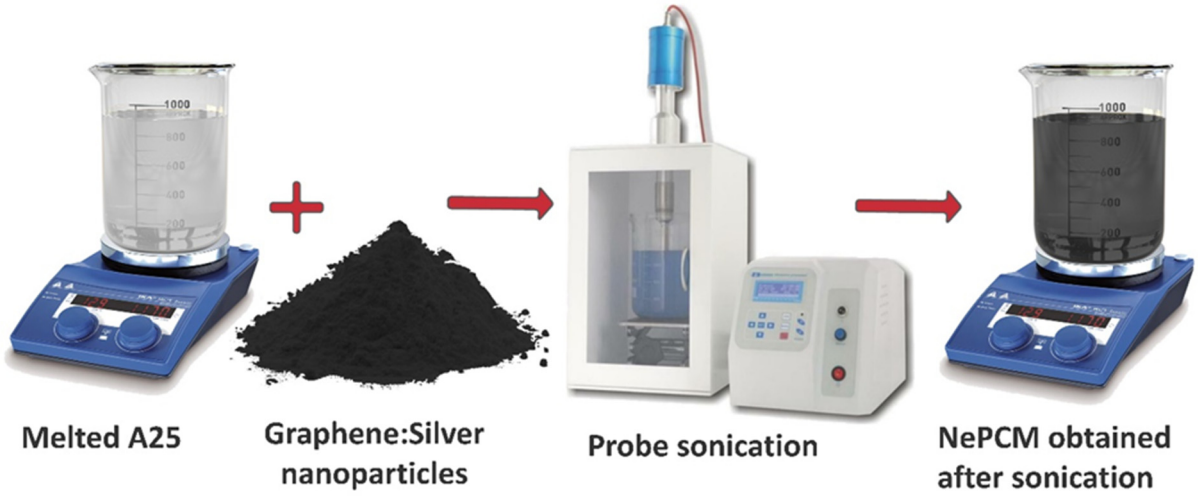

Figure 1. Synthesis route of hybrid nanocomposites.

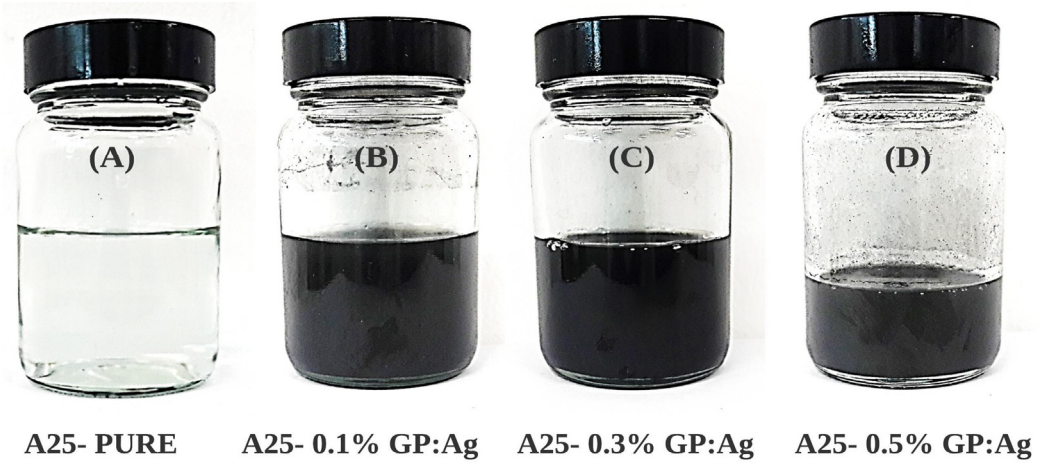

Figure 2. Images of pure and synthesized hybrid nanocomposites.

2.3. Characterization Techniques

The detailed morphology of Gp: Ag nanofillers was studied under field emission scanning electron microscopy (JSM-IT800, JEOL JAPAN, Tokyo, Japan) and transmission emission scanning electron microscopy (FEI Tecnai G2 20 S-TWIN, FEI Company, Hillsboro, OR, USA). The sample's thermal conductivity was estimated with a thermal property analyzer (model-TEMPOS, SH-3 sensor, Meter Group, Pullman, DC, USA). The latent heat and melting points were calculated using a differential scanning calorimeter analyzer (Model -DSC 822e, DSC-Mettler Toledo, Columbus, OH, USA). The thermal stability analysis of samples was conducted with a TGA (model-TGA 4000, Perkin Elmer, Waltham, MA, USA). The light ab-sorption ability of the HNePCMs was examined via a UV-VIS spectrometer (mod-el-LAMBDA 750, Perkin Elmer, Waltham, MA, USA). The changes in the attached functional group of synthesized HNePCMs were examined with Fourier transform infrared spec-troscopy (model-Spectrum Two FT-IR Spectrometer, Perkin Elmer, Waltham, MA, USA). A thermal imaging camera (model-S60, CAT, Irving, TX, USA) was used to capture infrared images of the samples.

2.4. Uncertainty Analysis

The reliability of the measurements performed was characterized by uncertainty analysis. Moreover, it also reflects the dispersion and accuracy of values measured. The uncertainties involved in direct measurement fall under random errors, named Class

A errors, and are measured by statistical methods. System errors are handled by non-statistical methods and are grouped as Class B errors. The uncertainty associated with the measurements can be estimated by the following equations and the associated terms [26]. The standard uncertainty of measured results is calculated according to specific rules for the A and B uncertainty of a particular measured value, which is commonly referred to as the combined uncertainty.

The mathematical expression gives class A uncertainty.

$$U_A(x) = \sqrt{\sum_{i=1}^{n} \frac{(X_i - X_{avg})^2}{n(n-1)}} \quad (1)$$

where n = total number of readings, X_{avg} = average value of the measurement

Under the same conditions, when x is measured multiple times, the standard uncertainty u(x) of x to be measured is obtained by combining the class A uncertainty $u_A(x)$ and the instrument uncertainty $u_{B2}(x)$.

$$u(x) = \sqrt{u_A{}^2(x) + u_{B2}{}^2(x)} \quad (2)$$

When a single measurement is performed on a physical quantity, the type B uncertainty is composed of the measurement uncertainty $u_{B1}(x)$ and the instrument uncertainty $u_{B2}(x)$.

The measurement uncertainty $u_{B1}(x)$ is caused by estimation, generally 1/10 or 1/5 of the scale value of the instrument.

Instrument uncertainty $u_{B2}(x)$ is determined by the characteristics of the instrument itself and is defined as:

$$u_{B2}(x) = \frac{a}{c} \quad (3)$$

where the confidence factor c can generally be processed with a uniform distribution, and the value assigned for c is $\sqrt{3}$.

For a single measurement x, the standard uncertainty u(x) of x to be measured is obtained by combining the class A uncertainty $u_{B1}(x)$ and the instrument uncertainty $u_{B2}(x)$.

$$u(x) = \sqrt{u_{B1}{}^2(x) + u_{B2}{}^2(x)} \quad (4)$$

$$x \pm u(x) \quad (5)$$

3. Results and Analysis

3.1. Morphological Analysis of Hybrid Nanoparticles

Figure 3 shows the FESEM images of hybrid graphene-silver nanofillers, which also shows the detailed structure of dispersed graphene sheets and silver nanomaterials. A few layers of transparent and thin graphene nanosheets were seen in the FESEM image (Figure 3A). Figure 3A shows that the graphene layers were arranged in a stacked pattern, overlapping each layer with another one in a folded manner [27]. From the FESEM image, the silver nanoparticles can be seen as a filler in between the graphene sheets. FESEM analysis shows that the graphene sheets got intercalated uniformly with silver nanomaterials. The silver nanomaterials lying on top of the graphene layers show a uniform and distinct contrast corresponding to the peripheral transparent graphene flakes (shown in Figure 3A). The TEM image of the HNePCM is given in Figure 3B. In addition, it can also be inferred that the intercalated silver nanomaterials in the graphene sheets may get oriented by interconnecting with each other [28], which eventually assists in linking the graphene flakes. This increases the thermally conducting path in the composite [29]. Standard morphological analysis techniques for low-temperature nanocomposites are not feasible as the phase transition temperature of these samples lies on the lower side. Moreover, the intense beam can readily melt the sample under inspection. Standard FESEM characterization of hybrid nanocomposites is impossible as the highly intense electron

beam melts the sample [30]. Energy dispersive x-ray (EDX) assessment was used to ensure the homogeneity of nanofillers and list the dominating elements. Figure 3C,D shows that nanoparticles had 77.79% of carbon (96.92 atomic) and 22.21% of silver (3.02% atomic). This clearly shows that both carbon and silver particles are present in the hybrid nanoparticle.

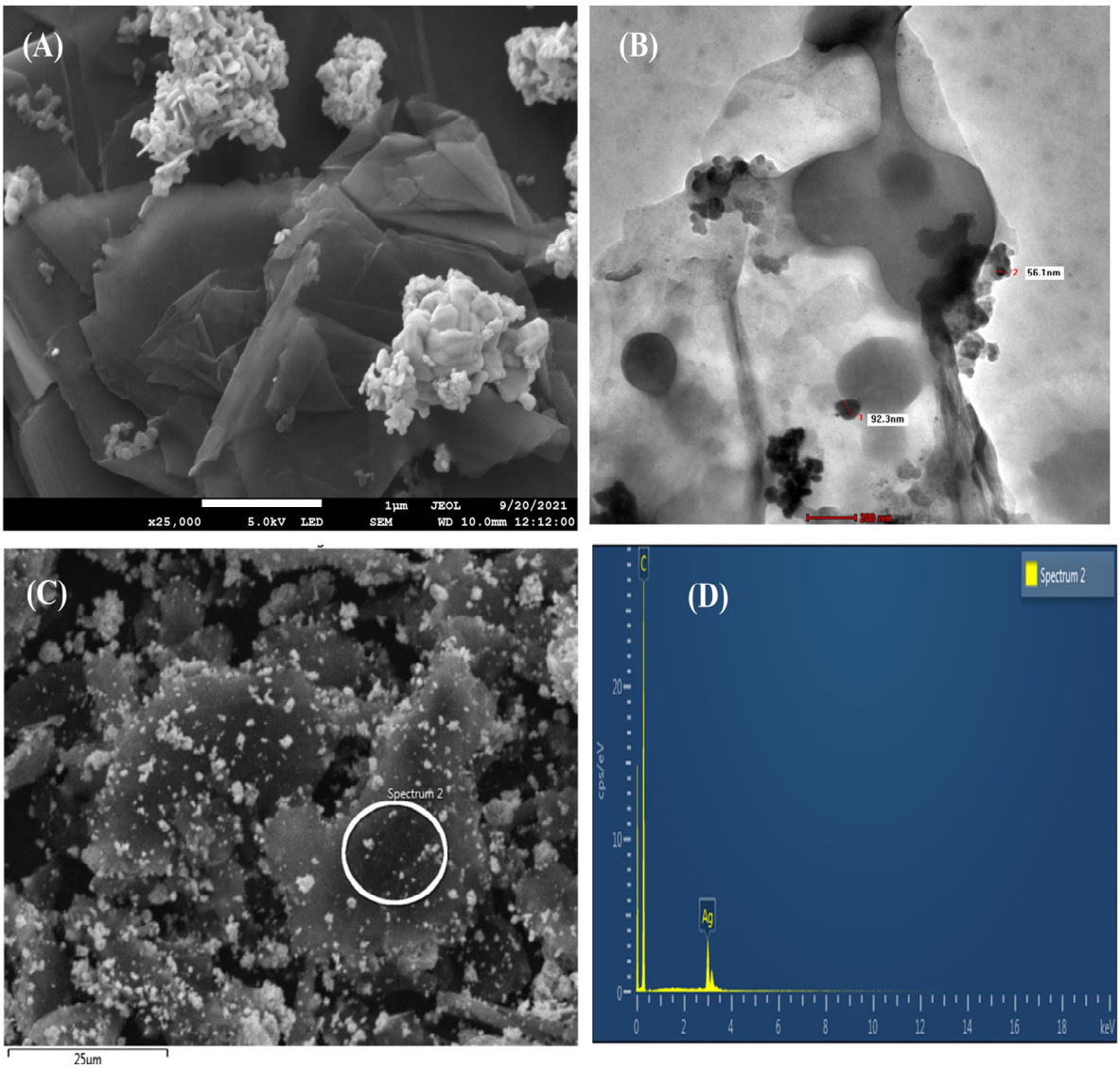

Figure 3. FESEM image of hybrid nanofillers (**A**) magnification 25,000 (**B**) TEM image of the HNePCMs (**C**,**D**) EDX mapping of hybrid nanoparticles.

3.2. FT-IR Spectrum Analysis of Hybrid Nanocomposites

The chemical structures of low-temperature pristine wax (A25) and the HNePCMs were studied with FTIR spectroscopy. Figure 4 details the FT-IR spectrum of all synthesized nanocomposites individually. The paraffin wax has an empirical formula of C_nH_{2n+2} and mainly holds three significant peaks of interest [17]. The occurrence of -CH_2- and -CH_3- groups in the composites were evident with the characteristic peak shifts [31]. The peaks within the range of 2800–3000 cm^{-1} indicate a symmetric stretching vibration of the -CH_2 and -CH_3 groups. Similarly, a peak in 1350–1470 region denotes the deformation of alkyl groups (-CH_3- and -CH_2-). Finally, the rocking motion of the -CH2- group is shown by the peak in 720–725 cm^{-1} region [32]. In the FT-IR spectrum, peaks are visible in the following wave numbers 2910 cm^{-1}, 2850 cm^{-1}, 1457 cm^{-1}, and 720 cm^{-1}. Both the peaks at 2910 cm^{-1} and 2850 cm^{-1} lie within the range of 2800–3000 cm^{-1}, showing

the symmetric stretching vibration of -CH_3- and -CH_2- groups. The peak 1457 cm^{-1} indicates the deformation of -CH2- and -CH3- groups, and lastly, the corresponding peak at 720 cm^{-1} denotes the rocking vibration of the -CH_2- group as it stays within the range of 720 cm^{-1}– 725 cm^{-1}. Paraffin holds a steady balance of attracting and opposing forces among carbon and hydrogen atoms which is clearly defined by the peaks [33]. Moreover, it is evident from the spectrum that all composites, even with varying loading rates of graphene/silver nanofillers, had similar characteristic peaks at the same wavenumbers (cm^{-1}). The dominant chemical structure of paraffin wax accounts for the uniformity in the FT-IR spectrum of all composites, even with different loading rates of nanofillers [34]. The FT-IR spectrum analysis revealed that no new peaks were present in the synthesized samples. Thus, the FT-IR results establish the absence of chemical reactions that alter the nature of paraffin during the synthesis of samples [35]. As no chemical reaction was present among the additives (paraffin, nanofillers, and surfactant), it can be concluded that the formulated samples were composites.

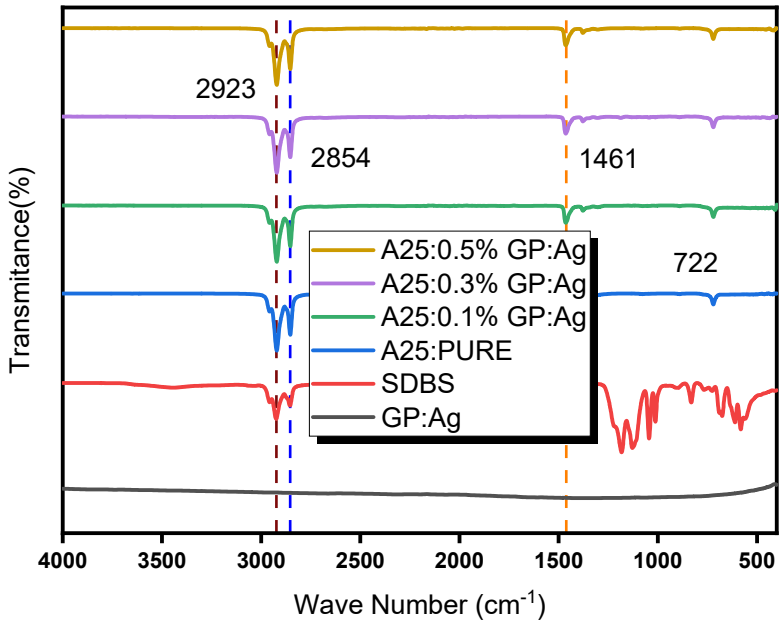

Figure 4. FTIR plot of base, nanoparticles, HNePCMs.

3.3. UV-Visible Spectrometer Spectrum Analysis of Nanocomposites

To analyze the light transmission capability of the synthesized hybrid nanocomposite, UV-Vis-NIR transmission spectra of paraffin and nanocomposites were plotted between 200 and 800 nm, as shown in Figure 5. The spectrum curve follows a simple principle which implies that it is impossible to have a material that simultaneously possesses both excellent absorbance and transmissibility. The transmissibility values remain inversely proportional to absorbance values for all samples [17]. The light transmission capability of the hybrid nanocomposite showed a declining trend with the rise in the dispersion of hybrid nanofillers. The improved light absorption of the nanofillers accounts for this trend. In contrast with pure paraffin, hybrid nanocomposites exhibited an entire absorbance of solar radiation throughout the UV-Vis-NIR range. Pure paraffin had an absorbance of 13.22%, and samples with 0.1%, 0.3%, and 0.5% nano fillers exhibited a corresponding absorbance of 97.35%, 99.99%, and 99.75%, respectively. The absorption spectrum was calculated using the solar spectrum data provided by NREL [36]. Moreover, the distinct absorption characteristic of hybrid graphene–silver nanoflakes as the supporting material, enables the nanocomposite to harvest the maximum solar energy. This is because of the firm absorption peaks of the nanocomposite at 245 nm, where most of the solar energy gets distributed (consisting of 7% UV, 50% visible, and 43% infrared) [37]. However,

the nanocomposite exhibits total absorption over the entire UV-Vis-NIR range. Solar transmission of nanocomposites in different spectrums are summarized in Table 2. The spectrum analysis results lie in tandem with the physical appearance of paraffin (white) and hybrid nanocomposite (black). The nanosheets function as a perfect black body because of their effective light scattering and trapping ability, enhancing photoabsorption and imparting thermal energy to the wax in the hybrid nanocomposites. With a linear rise in the loading rate of nanofillers, the amount of solar energy absorbed from solar radiation rises, improving the composite's application range, especially in ambient temperature, direct solar thermal applications, such as building thermal management.

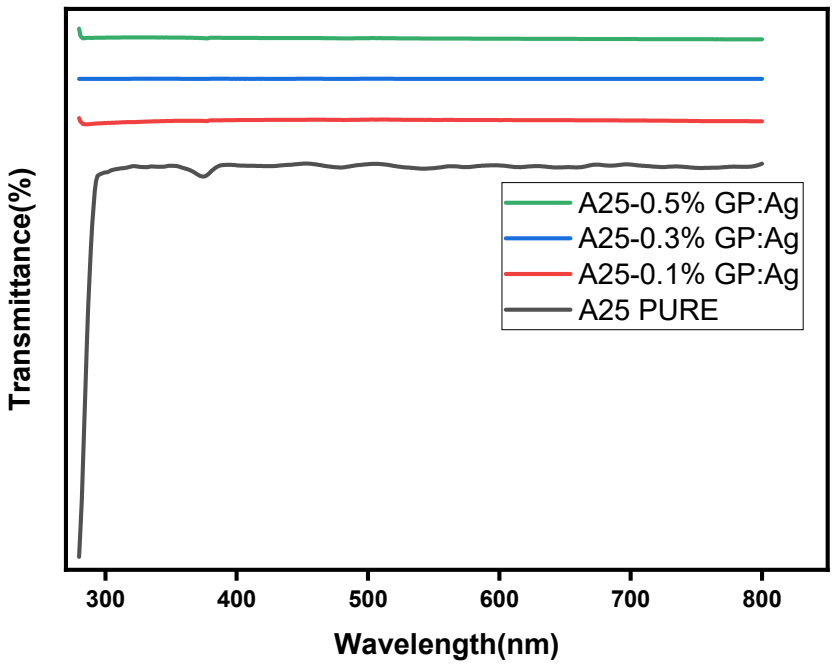

Figure 5. Light transmittance spectrum of samples.

Table 2. Solar transmission of nanocomposites in different spectrums.

SAMPLE	TOTAL	UV	VISIBLE	IR	Reference
SOLAR spectrum	100%	7%	50%	43%	[37]
A25-0.0%	86.78%	6.28%	80.63%	13.09%	Current work
A25-0.1%	2.65%	5.88%	81.73%	12.39%	Current work
A25-0.3%	0.01%	0%	78.03%	21.97%	Current work
A25-0.5%	0.25%	2.51%	76.13%	21.37%	Current work

3.4. Thermal Stability of Paraffin/Graphene: Silver Nanocomposites

The thermal stability of nanocomposites is also pivotal, especially for LHES applications. In this experimental work, the thermal stability of A25 as PCM dispersed with different loading rates of graphene–silver additive was assessed using thermogravimetric analysis (TGA) and derivative thermogravimetry (DTG). Figure 6 displays TGA, and Figure 7 DTG curves of A25 and A25/ graphene–silver nanocomposite with different loading rates of nano additives. The weight loss (5 wt%) and the corresponding temperatures at ($T_{5\%}$) are summarized in Table 3. The temperature at which the maximal weight loss rate (T_{max}) happens is evaluated using DTG curves. The TGA curves show that the base PCM and even the formulated hybrid nanocomposites had a single-step degradation. The samples recorded negligible weight loss in the 30–155 °C. The formulated nanocomposite had excellent thermal stability even at 155 °C, which lies well above the peak melting temperature of pure A25 (25 °C). Higher thermal stability (above the working temperature

area) is one of the mandatory prerequisites for a PCM to be deployed for TES. As temperature surpassed 155 °C, A25 in the composite started decomposition and eventually halted at 266 °C, as shown in Figure 7. Furthermore, the heat resistance index [38] (THRI) was calculated by the following mathematical expression.

$$\text{THRI} = 0.49 \times [T_{5\%} + 0.6 \times (T_{30\%} - T_{5\%})] \quad (6)$$

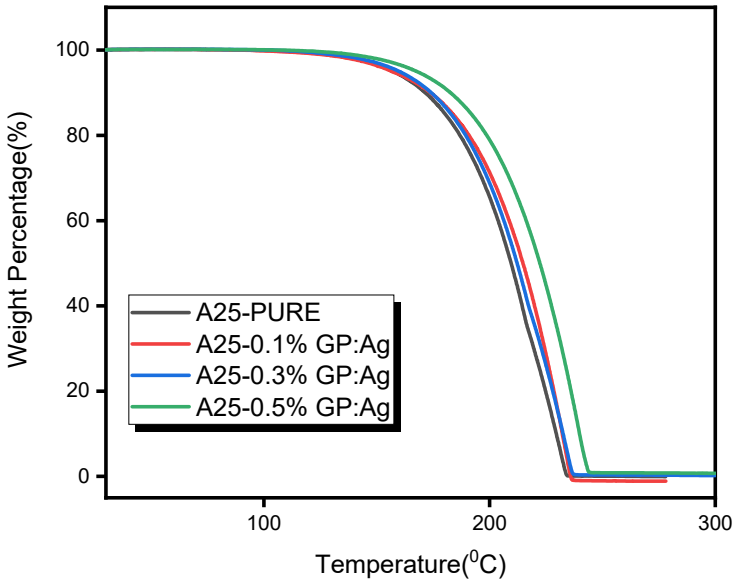

Figure 6. TGA thermograms of A25 and hybrid nanocomposites.

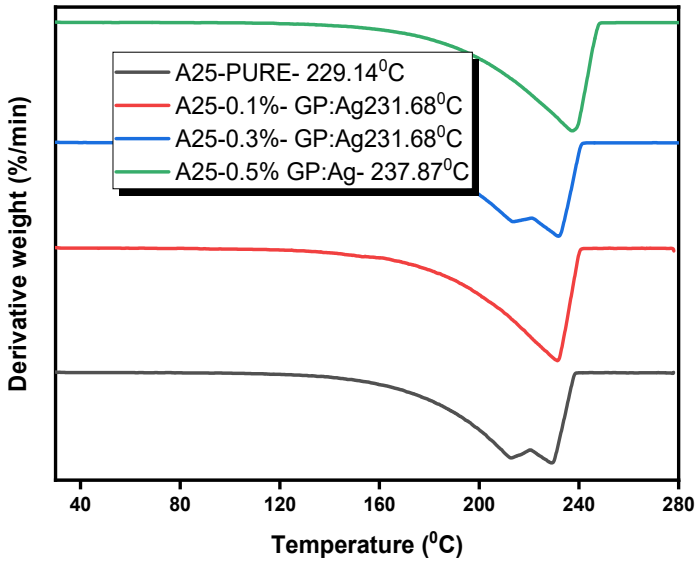

Figure 7. DTG thermograms of A25 and hybrid nanocomposites.

Table 3. Thermal stability parameters of hybrid nanocomposites.

Samples	$T_{5\%}$ (°C)	$T_{30\%}$ (°C)	T_{max} (°C)	Heat Resistance Index (°C)
A25-0.0%	157.37	196.57	229.14	88.63610
A25-0.1%	156.73	201.1	231.68	89.84248
A25-0.3%	159.92	199.11	231.68	89.88266
A25-0.5%	167.96	208.73	237.87	94.28678

The heat resistance index of all samples was tabulated in Table 4. The THRI slightly improved with the addition of nanofillers. This is because nanofillers replace a portion of the PCM matrix. The value almost remains constant for nanocomposites. The temperature readings at which a maximal weight loss rate forA25 and nanocomposite was recorded are 229.14 °C (A25-0%), 231.68 °C (A25-0.1%), 231.68 °C (A25-0.3%), and 237.87 °C (A25-0.5%). These readings could be referred to as the decomposition of paraffin. When compared with pure A25, the decomposition temperatures (the temperature at which maximal weight loss rate) for hybrid nanocomposite were higher than that of A25, which showed the dispersion of Gp. Ag additives enhanced the thermal stability of nanocomposites. The maximum temperature of weight loss of the hybrid nanocomposites was 2–7 °C more than pure A25. In addition, it was also found that the rate of weight loss of the hybrid nanocomposite was comparatively sluggish compared to A25. It is worth mentioning that the synthesized nanocomposites had both improved stability and heat resistance compared to pure A25.

3.5. Effect of Graphene: Silver Dispersion on the Thermal Behavior of Hybrid Nanocomposites

Latent-heat and phase transition temperatures during the phase transition of pristine A25 and HNePCMs were evaluated using a DSC. The numerical values of thermal properties were evaluated using DSC are detailed in Table 4. The tabulated values show that the dispersion of hybrid nanofillers slightly altered the thermal properties of the nanocomposites. The DSC thermograms of all composites had a similar shape which showed that A25 had zero transformation during the synthesis of nanocomposites. Figure 8 illustrates the melting and freezing enthalpies, melting and freezing points of HNePCMs during the phase transition process. Moreover, the enthalpy of melting and freezing of all hybrid composites was found to have increased with the dispersion of hybrid nanofillers. The maximal enhancement in melting latent heat of hybrid nanocomposites was 6.6%, for A25-0.3%, as compared with pure A25. Similarly, the maximal boost in solidification latent heat was 8.4% for the 0.3% sample. The latent heat shows a linear increment with a rise in the dispersion rate of hybrid nano additives. Nanocomposites possess an ultra-thin surface with negligible thickness, resulting in a nearly zero aspect ratio of graphene sheets. Large specific areas and Van Der Waals attraction tend to form aggregate formation. The smaller size of nano additives also means that their molecular density is also high. The rise in latent heat is attributed to a larger surface area of nano additives which further enhances the intermolecular attraction [39].

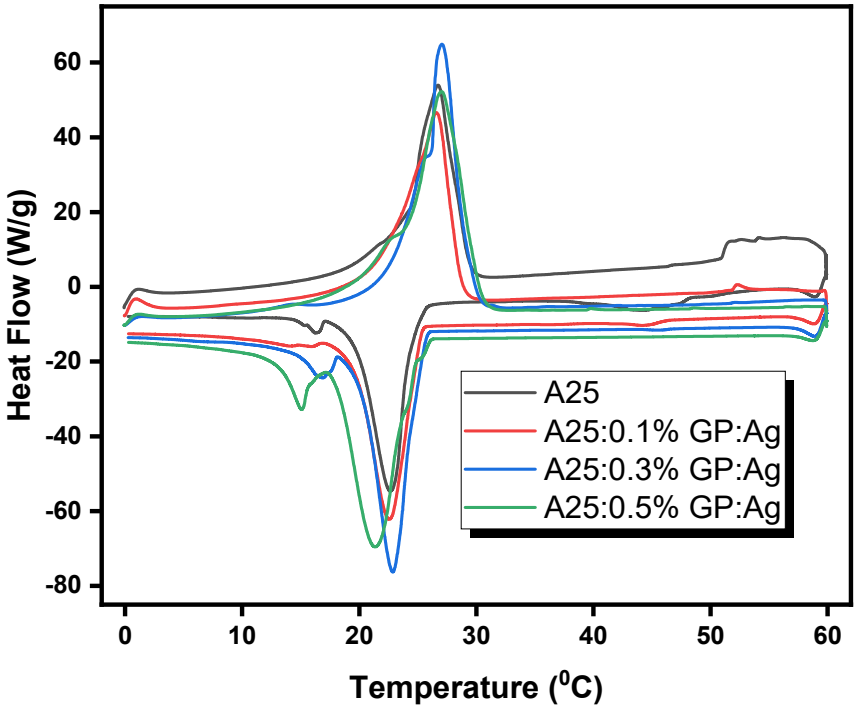

Figure 8. DSC thermogram of samples.

Table 4. Melting and freezing point of composites.

Sample	Enthalpy of Melting ΔH_m (J/g)	Melting Point T_m (°C)	Enthalpy of Freezing ΔH_f (J/g)	Freezing Point T_f (°C)	Degree of Supercooling (°C)	Heat Storage Efficiency γ (%)
A25-0.0%	253.52	26.72	241.98	22.68	4.04	4.55
A25-0.1%	265.75	26.60	253.32	22.58	4.02	4.68
A25-0.3%	270.32	27.07	262.36	22.86	4.21	2.94
A25-0.5%	269.90	27.03	256.40	21.38	5.65	5.00

Furthermore, both the endothermic and exothermic peaks of all synthesized HNePCMs are observed to be narrower/sharper than pristine A25. This is mainly due to the establishment of a thermally conducting network with the dispersion of hybrid nanofillers, providing a rapid thermally conducting path throughout the composite. This eventually promoted the heat transfer rate in the hybrid nanocomposite. Thus, the pace of phase transfer of hybrid nanocomposites will rise, thereby causing a rapid melting and freezing of HNePCMs. It is also noted that both the melting and freezing temperatures show a slight variation mainly due to the rise in λ value of the composites. In this connection, enhancing the loading rate of nanofillers further enhances the heat transfer performance. To assess the phase change performance of synthesized HNePCMs, a typical parameter termed heat storage efficiency (γ) was used. The following mathematical relation is used to estimate (γ).

$$\gamma = \left(1 - \frac{h_f}{h_m}\right) \times 100\% \quad (7)$$

where h_f denotes the enthalpy of freezing and h_m denotes the enthalpy of melting of the samples. The heat loss percentage of entire HNePCMs showed changes within a permissible limit during the cyclic endothermic and exothermic process. The quality loss that occurred while melting during the DSC test accounts for a higher enthalpy of melting for A25 (as compared with freezing enthalpy) and the prepared nanocomposite.

3.6. Thermal Conductivity of Hybrid Nanocomposites

In thermal management applications, the primary function of PCM is to effectively store and release the generated thermal energy using its phase transition ability. The poor λ value of pristine PCMs dampens both the heat storage and release rate, thereby restricting its application range. A PCM having an enhanced thermal conductivity value raises the rate of heat transfer during the phase transition process, which eventually shortens the time for melting and solidification [40]. In this study, among all the synthesized composites, (A25-0.3%) clocked a maximal λ value of 0.395 W/mK (detailed in Table 5). The increment in λ value with hybrid nanofiller infusion could be detailed by two mechanisms, namely the synergy effect and interfacial thermal resistance. The synergy effect (evaluated by synergistic factor η) is strong in the composites, which predominantly forms an effective thermal conductive layer, improving thermal conductivity. The nanoparticle dispersion lowers the interfacial thermal resistance and improves thermal conductivity [41]. The reagglomeration caused by the dispersion of nanofillers also supports the enhancement of λ value.

Table 5. Thermal Conductivity of composites in solid-state.

Sample	Thermal Conductivity of Composites (W/mK)	Enhancement in Thermal Conductivity (%)
A25-0.0%	0.208 ± 0.029	----
A25-0.1%	0.242 ± 0.029	16.44
A25-0.3%	0.395 ± 0.029	89.88
A25-0.5%	0.290 ± 0.029	55.42

The excellent λ value of graphene sheets could be the root cause of a boost in of λ value of hybrid nanocomposite [42]. The nanofillers hold an ultra-thin surface with a negligible thickness, resulting in an almost zero aspect ratio of graphene sheets [43]. A percolating thermally conductive network could be generated in the PCM matrix with graphene sheets having these features. Furthermore, a tunnelling impact that occurs among adjoining graphene sheets also assists in boosting the λ value of samples. The graphene sheets form an entire conductive network by contacting the adjacent nanosheets in percolation, and a substantial increment in the amount of graphene sheets raises the number of conducting networks until the conductivity levels show a decline [44]. Graphene holds an inherent ability to generate an uninterrupted, thermally conductive chain mainly because of its negligible aspect ratio, which improves thermal conductivity [45].

Furthermore, the hybrid nanoparticles connect within the PCM matrix, as graphene sheets exist along with spherical-shaped silver nanofillers [29]. The electrons jump in between adjacent graphene sheets in the matrix with the assistance of silver nanomaterials. Hence, the nanocomposite possesses a stronger energy transport within the matrix [46]. The impact of interfacial thermal resistance between hybrid Gp-Ag nanofillers and PCM matrix cannot be overrated in solid-state nanocomposites. The interfacial thermal boundary resistance could hinder the enrichment of λ value in nanocomposites. This is mainly because the dimensionality of nanofillers is intensified based on the results for 2-D materials, including graphene nanoflakes [47]. The nanocomposites had maximal thermal conductivity at 0.3 Wt%, corresponding to an 89.88% rise. The conductivity further slips to 0.290 W/mK at 0.5 wt%, which shows only an increment of 55.42%. As the nanofiller dispersion crosses the 0.3 Wt% mark, thermal conductivity shows a declining trend. A maximum of 89.88% and a minimum of 16.44% improvement in λ value are obtained with the addition of Gp-Ag nanofillers in wax (shown in Figure 9). The decline in λ value with a rise in nanofiller loading is mainly because (1) the thermal network gets broken down because of the agglomeration of hybrid nanofillers; (2) an increment in phonon-impurity (nanofillers) scattering as the loading rate of nanofillers rises; and (3) finally, a synergic effect of both thermal network crackdown and rise in scattering.

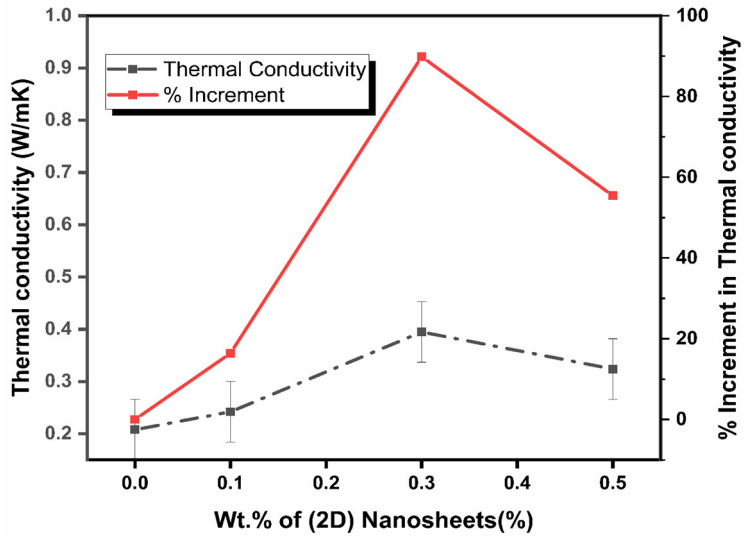

Figure 9. Solid-state thermal conductivity of samples.

3.7. Infrared Thermal Imaging

The surface temperature distribution of pure and HNePCMs at various time stamps during the melting process are detailed in Figure 10 (IR thermal images of pristine and HNePCMs). The change in temperature of the samples could be noted from the color pattern, which denotes a lower to higher temperature transition using colors ranging from blue to red. The uniform melting of all samples was noted at a constant temperature. The HNePCM composite displayed both rapid heat absorption and thermal management when compared with pure A25 PCM under each moment due to dispersed hybrid nanofillers, indicating an incredible temperature and time-regulating ability during the heating process. Figure 10 shows that the HNePCMs logged a higher temperature at every timestamp when compared with pure A25. This indicates that the sample's overall thermal absorption and transfer ability improve with a rise in nanofiller content, and it could be effectively used in building thermal management.

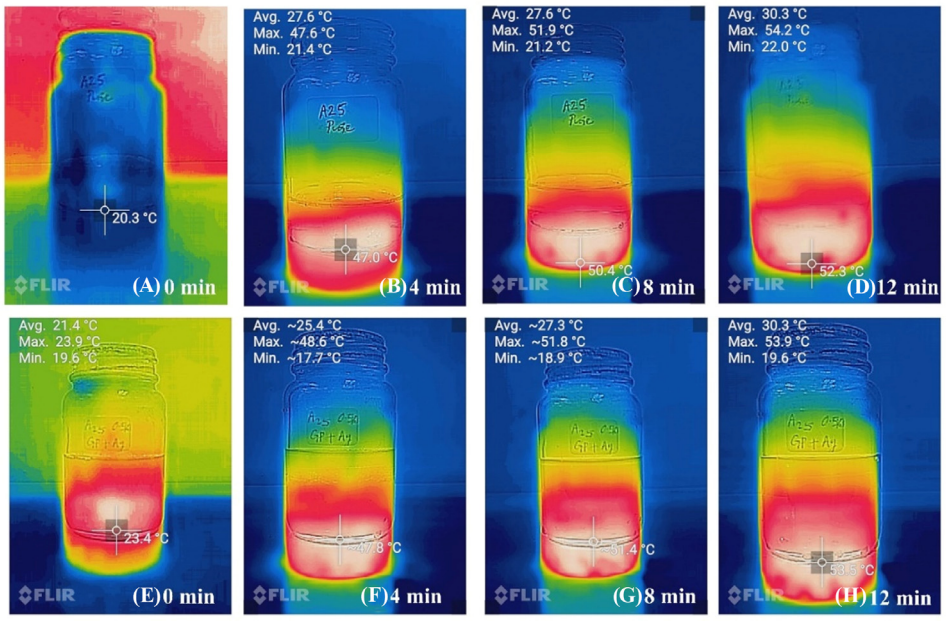

Figure 10. (**A**–**D**) IR images of pure A25, (**E**–**H**) IR image of HNePCM.

4. Conclusions

In this experimental work, hybrid nanocomposite phase change materials were produced by dispersing hybrid graphene–silver nanofillers in paraffin wax (A25H) by a two-step method. The primary goal of the experiment was to boost the optical and thermophysical characteristics, particularly thermal conductivity (which is still essential in thermal energy storage applications) for building thermal management. A comparative summary of thermophysical properties of paraffin-based nanocomposites dispersed with different dimensional nanofillers is presented in Table 1. The thermophysical characterization results and its trends clearly state that the synthesized composite is homogenous. To the best of our knowledge, the synthesis of HNePCM loaded with 2-D graphene–silver nanofillers in low-temperature paraffin and its detailed thermophysical characterization remains a novel work. An in depth thermophysical characterization of the novel hybrid nanocomposite at solid state was conducted, and the crucial results are summarized below:

(1) The novel hybrid nano-enhanced composite phase change material logged an increment in enthalpy in comparison with base (6.7%). An increment in enthalpy for nanocomposite is preferable as it can retain more heat, even with the same amount of PCM.
(2) Thermal conductivity was increase by a maximum of 90% with the dispersion of graphene: silver nanofillers (0.3 wt%). Enrichment in thermal conductivity causes a drop in interfacial thermal resistance, and this improves the charging efficiency of HNePCM when used for thermal energy storage.
(3) The pure paraffin had a maximal solar transmissivity of around 87%, and the A25-0.3% sample (0.3% nanofiller loaded) clocked a maximum transmissivity of 0.01%. This result shows that the hybrid nanocomposite could be used in shielding UV rays.
(4) The thermal stability of the composites was also enhanced with the nanofiller infusion. A maximum increment of 5.7 °C was found in THRI results.
(5) Moreover, FT-IR results confirm that the synthesized samples were composites.

The outlined thermophysical characterization results justify an enrichment in thermophysical properties, particularly λ value, optical property, enthalpy, and finally, thermal stability. In addition, the hybrid nanocomposite also had good thermal energy storage capability. The melting and freezing points of the samples lie in the range of 21–27 °C. The fabricated composite could be used for different applications, e.g., the thermal management of PV panels, buildings, etc. This work may provide new insights for fabricating hybrid nanocomposites, presenting broader applications with highly thermally conductive and solar spectrum absorptive capabilities. Finally, with the addition of graphene–silver hybrid nanofillers to low-temperature paraffin, next-generation hybrid composites with improved heat storage and solar absorptivity were synthesized successfully.

Author Contributions: Conceptualization, J.P.; methodology, J.P. and A.K.P.; writing—original draft, J.P. and A.K.P.; funding acquisition, K.K., A.K.P. and M.S.; formal analysis, J.P., A.K.P. and V.V.T.; supervision, K.K., M.S. and A.K.P.; project administration, K.K., M.S. and A.K.P.; writing—review & editing, A.K.P. and V.V.T. All authors have read and agreed to the published version of the manuscript.

Funding: The work is funded by Universiti Malaysia Pahang under RDU213303 and Doctoral Research Scheme. We also received financial aid from Sunway University via Sunway University's Internal Grant Scheme (IGS) 2022 (GRTIN-IGS-RCNMET[S]-15-2022).

Institutional Review Board Statement: Not applicable.

Informed Consent Statement: Not applicable.

Data Availability Statement: The data presented in current work is available within this article.

Conflicts of Interest: The authors declare no conflict of interest.

References

1. Cui, Y.; Zhu, J.; Zhang, F.; Shao, Y.; Xue, Y. Current Status and Future Development of Hybrid PV/T System with PCM Module: 4E (Energy, Exergy, Economic and Environmental) Assessments. *Renew. Sustain. Energy Rev.* **2022**, *158*, 112147. [CrossRef]
2. Du, R.; Wu, Y.; Yang, Y.; Zhai, T.; Zhou, T.; Shang, Q.; Zhu, L.; Shang, C.; Guo, Z. Porosity Engineering of MOF-Based Materials for Electrochemical Energy Storage. *Adv. Energy Mater.* **2021**, *2100154*, 2100154. [CrossRef]
3. Jacob, J.; Pandey, A.K.; Rahim, N.A.; Selvaraj, J.; Samykano, M.; Saidur, R.; Tyagi, V.V. Concentrated Photovoltaic Thermal (CPVT) Systems: Recent Advancements in Clean Energy Applications, Thermal Management and Storage. *J. Energy Storage* **2022**, *45*, 103369. [CrossRef]
4. Ismail, K.A.R.; Lino, F.A.M.; Teggar, M.; Arıcı, M.; Machado, P.L.O.; Alves, T.A.; De Paula, A.C.O.; Benhorma, A. A Comprehensive Review on Phase Change Materials and Applications in Buildings and Components. *ASME Open J. Eng.* **2022**, *1*, 011049 .
5. Cheng, P.; Chen, X.; Gao, H.; Zhang, X.; Tang, Z.; Li, A.; Wang, G. Different Dimensional Nanoadditives for Thermal Conductivity Enhancement of Phase Change Materials: Fundamentals and Applications. *Nano Energy* **2021**, *85*, 105948. [CrossRef]
6. Zhang, N.; Yuan, Y.; Cao, X.; Du, Y.; Zhang, Z.; Gui, Y. Latent Heat Thermal Energy Storage Systems with Solid–Liquid Phase Change Materials: A Review. *Adv. Eng. Mater.* **2018**, *20*, 1–30. [CrossRef]
7. D'Oliveira, E.J.; Pereira, S.C.C.; Groulx, D.; Azimov, U. Thermophysical Properties of Nano-Enhanced Phase Change Materials for Domestic Heating Applications. *J. Energy Storage* **2022**, *46*, 103794. [CrossRef]
8. Magendran, S.S.; Khan, F.S.A.; Mubarak, N.M.; Vaka, M.; Walvekar, R.; Khalid, M.; Abdullah, E.C.; Nizamuddin, S.; Karri, R.R. Synthesis of Organic Phase Change Materials (PCM) for Energy Storage Applications: A Review. *Nano-Struct. Nano-Objects* **2019**, *20*, 100399. [CrossRef]
9. Martín, M.; Villalba, A.; Fernández, A.I.; Barreneche, C. Energy & Buildings Development of New Nano-Enhanced Phase Change Materials (NEPCM) to Improve Energy Efficiency in Buildings: Lab-Scale Characterization. *Energy Build.* **2019**, *192*, 75–83. [CrossRef]
10. Paul, J.; Kadirgama, K.; Samykano, M.; Pandey, A.K.; Tyagi, V.V. A Comprehensive Review on Thermophysical Properties and Solar Thermal Applications of Organic Nano Composite Phase Change Materials. *J. Energy Storage* **2022**, *45*, 103415. [CrossRef]
11. Leong, K.Y.; Abdul Rahman, M.R.; Gurunathan, B.A. Nano-Enhanced Phase Change Materials: A Review of Thermo-Physical Properties, Applications and Challenges. *J. Energy Storage* **2019**, *21*, 18–31. [CrossRef]
12. Chen, L.; Zou, R.; Xia, W.; Liu, Z.; Shang, Y.; Zhu, J.; Wang, Y.; Lin, J.; Xia, D.; Cao, A. Electro- and Photodriven Phase Change Composites Based on Wax-Infiltrated Carbon Nanotube Sponges. *ACS Nano* **2012**, *6*, 10884–10892. [CrossRef]
13. Ma, T.; Liu, Z.; Wen, J.; Gao, Y.; Ren, X.; Chen, H.; Jin, C.; Ma, X.L.; Xu, N.; Cheng, H.M.; et al. Tailoring the Thermal and Electrical Transport Properties of Graphene Films by Grain Size Engineering. *Nat. Commun.* **2017**, *8*, 1–9. [CrossRef] [PubMed]
14. Kargar, F.; Barani, Z.; Salgado, R.; Debnath, B.; Lewis, J.S.; Aytan, E.; Lake, R.K.; Balandin, A.A. Thermal Percolation Threshold and Thermal Properties of Composites with High Loading of Graphene and Boron Nitride Fillers. *ACS Appl. Mater. Interfaces* **2018**, *10*, 37555–37565. [CrossRef] [PubMed]
15. Zheng, R.; Gao, J.; Wang, J.; Chen, G. Reversible Temperature Regulation of Electrical and Thermal Conductivity Using Liquid-Solid Phase Transitions. *Nat. Commun.* **2011**, *2*, 289. [CrossRef]
16. Suresh, C.; Kumar Hotta, T.; Saha, S.K. Phase Change Material Incorporation Techniques in Building Envelopes for Enhancing the Building Thermal Comfort-A Review. *Energy Build.* **2022**, *268*, 112225. [CrossRef]
17. George, M.; Pandey, A.K.; Abd, N.; Tyagi, V.V.; Shahabuddin, S.; Saidur, R. A Novel Polyaniline (PANI)/Para Ffi n Wax Nano Composite Phase Change Material: Superior Transition Heat Storage Capacity, Thermal Conductivity and Thermal Reliability. *Sol. Energy* **2020**, *204*, 448–458. [CrossRef]
18. Habib, N.A.; Ali, A.J.; Chaichan, M.T.; Kareem, M. Carbon Nanotubes/Paraffin Wax Nanocomposite for Improving the Performance of a Solar Air Heating System. *Therm. Sci. Eng. Prog.* **2021**, *23*, 100877. [CrossRef]
19. Sheng, N.; Rao, Z.; Zhu, C.; Habazaki, H. Honeycomb Carbon Fibers Strengthened Composite Phase Change Materials for Superior Thermal Energy Storage. *Appl. Therm. Eng.* **2020**, *164*, 114493. [CrossRef]
20. Joseph, M.; Sajith, V. Graphene Enhanced Paraffin Nanocomposite Based Hybrid Cooling System for Thermal Management of Electronics. *Appl. Therm. Eng.* **2019**, *163*, 114342. [CrossRef]
21. Aslfattahi, N.; Saidur, R.; Arifutzzaman, A.; Sadri, R.; Bimbo, N.; Sabri, M.F.M.; Maughan, P.A.; Bouscarrat, L.; Dawson, R.J.; Said, S.M.; et al. Experimental Investigation of Energy Storage Properties and Thermal Conductivity of a Novel Organic Phase Change Material/MXene as A New Class of Nanocomposites. *J. Energy Storage* **2020**, *27*, 101115. [CrossRef]
22. Paul, J.; Pandey, A.K.; Mishra, Y.N.; Said, Z.; Mishra, Y.K.; Ma, Z.; Jacob, J.; Kadirgama, K.; Samykano, M.; Tyagi, V.V. Nano-Enhanced Organic Form Stable PCMs for Medium Temperature Solar Thermal Energy Harvesting: Recent Progresses, Challenges, and Opportunities. *Renew. Sustain. Energy Rev.* **2022**, *161*, 112321. [CrossRef]
23. Wang, J.; Xie, H.; Xin, Z. Thermal Properties of Paraffin Based Composites Containing Multi-Walled Carbon Nanotubes. *Thermochim. Acta* **2009**, *488*, 39–42. [CrossRef]
24. B, K.; Pandey, A.K.; Shahabuddin, S.; George, M.; Sharma, K.; Samykano, M.; Tyagi, V.V.; Saidur, R. Synthesis and Characterization of Conducting Polyaniline@cobalt-Paraffin Wax Nanocomposite as Nano-Phase Change Material: Enhanced Thermophysical Properties. *Renew. Energy* **2021**, *173*, 1057–1069. [CrossRef]
25. Li, M. A Nano-Graphite/Paraffin Phase Change Material with High Thermal Conductivity. *Appl. Energy* **2013**, *106*, 25–30. [CrossRef]

26. Sun, L.; Diao, R.; Yang, F.; Lin, B. Analysis of the Thermal Performance of the Embedded Composite Phase Change Energy Storage Wall. *ACS Omega* **2020**, *5*, 17005–17021. [CrossRef] [PubMed]
27. Wang, S.; Wang, C.; Ji, X. Towards Understanding the Salt-Intercalation Exfoliation of Graphite into Graphene. *RSC Adv.* **2017**, *7*, 52252–52260. [CrossRef]
28. Ramesh, B.P.; Blau, W.J.; Tyagi, P.K.; Misra, D.S.; Ali, N.; Gracio, J.; Cabral, G.; Titus, E. Thermogravimetric Analysis of Cobalt-Filled Carbon Nanotubes Deposited by Chemical Vapour Deposition. *Thin Solid Films* **2006**, *494*, 128–132. [CrossRef]
29. Cheng, C.; Li, D. Solvated Graphenes: An Emerging Class of Functional Soft Materials. *Adv. Mater.* **2013**, *25*, 13–30. [CrossRef] [PubMed]
30. Jacob, J.; Pandey, A.K.; Rahim, N.A.; Selvaraj, J.; Paul, J.; Samykano, M.; Saidur, R. Quantifying Thermophysical Properties, Characterization, and Thermal Cycle Testing of Nano-Enhanced Organic Eutectic Phase Change Materials for Thermal Energy Storage Applications. *Sol. Energy Mater. Sol. Cells* **2022**, *248*, 112008. [CrossRef]
31. Aslfattahi, N.; Saidur, R.; Arifutzzaman, A.; Abdelrazik, A.S.; Samylingam, L.; Sabri, M.F.M.; Sidik, N.A.C. Improved Thermo-Physical Properties and Energy Efficiency of Hybrid PCM/Graphene-Silver Nanocomposite in a Hybrid CPV/Thermal Solar System. *J. Therm. Anal. Calorim.* **2022**, *147*, 1125–1142. [CrossRef]
32. Mekaddem, N.; Ali, S.B.; Fois, M.; Hannachi, A. Paraffin/Expanded Perlite/Plaster as Thermal Energy Storage Composite. *Energy Procedia* **2019**, *157*, 1118–1129. [CrossRef]
33. Allahyarzadeh, V.; Montazer, M.; Nejad, N.H.; Samadi, N. In Situ Synthesis of Nano Silver on Polyester Using NaOH/Nano TiO 2. *J. Appl. Polym. Sci.* **2013**, *129*, 892–900. [CrossRef]
34. Kim, C.H.; Joo, C.K.; Chun, H.J.; Yoo, B.R.; Noh, D.I.; Shim, Y.B. Instrumental Studies on Silicone Oil Adsorption to the Surface of Intraocular Lenses. *Appl. Surf. Sci.* **2012**, *262*, 146–152. [CrossRef]
35. Mansur, H.S.; Oréfice, R.L.; Mansur, A.A.P. Characterization of Poly(Vinyl Alcohol)/Poly(Ethylene Glycol) Hydrogels and PVA-Derived Hybrids by Small-Angle X-Ray Scattering and FTIR Spectroscopy. *Polymer* **2004**, *45*, 7193–7202. [CrossRef]
36. Gueymard, C.A. The Sun's Total and Spectral Irradiance for Solar Energy Applications and Solar Radiation Models. *Sol. Energy* **2004**, *76*, 423–453. [CrossRef]
37. Wang, J.; Li, Y.; Deng, L.; Wei, N.; Weng, Y.; Dong, S.; Qi, D.; Qiu, J.; Chen, X.; Wu, T. High-Performance Photothermal Conversion of Narrow-Bandgap Ti2O3Nanoparticles. *Adv. Mater.* **2017**, *29*, 1–6. [CrossRef]
38. Yang, Z.; Mao, Z.; Xiang, B.; Zhang, J. Construction of a Binary Channel Efficient Cooling Composites with Reflective and Phase-Change Properties. *Compos. Part B Eng.* **2019**, *178*, 107517. [CrossRef]
39. Shaikh, S.; Lafdi, K.; Hallinan, K. Carbon Nanoadditives to Enhance Latent Energy Storage of Phase Change Materials. *J. Appl. Phys.* **2008**, *103*, 094302. [CrossRef]
40. Arshad, A.; Jabbal, M.; Yan, Y. Preparation and Characteristics Evaluation of Mono and Hybrid Nano-Enhanced Phase Change Materials (NePCMs) for Thermal Management of Microelectronics. *Energy Convers. Manag.* **2020**, *205*, 112444. [CrossRef]
41. Qu, Y.; Wang, S.; Zhou, D.; Tian, Y. Experimental Study on Thermal Conductivity of Paraffin-Based Shape-Stabilized Phase Change Material with Hybrid Carbon Nano-Additives. *Renew. Energy* **2020**, *146*, 2637–2645. [CrossRef]
42. Balandin, A.A.; Ghosh, S.; Bao, W.; Calizo, I.; Teweldebrhan, D.; Miao, F.; Lau, C.N. Superior Thermal Conductivity of Single-Layer Graphene. *Nano Lett.* **2008**, *8*, 902–907. [CrossRef] [PubMed]
43. Shahil, K.M.F.; Balandin, A.A. Graphene-Multilayer Graphene Nanocomposites as Highly Efficient Thermal Interface Materials. *Nano Lett.* **2012**, *12*, 861–867. [CrossRef] [PubMed]
44. Sadasivuni, K.K.; Ponnamma, D.; Kim, J.; Thomas, S. Graphene-Based Polymer Nanocomposites in Electronics. In *Graphene-Based Polymer Nanocomposites in Electronics*; Sadasivuni, K.K., Ponnamma, D., Kim, J., Sabu, T., Eds.; Springer International Publishing: Berlin/Heidelberg, Germany, 2015; pp. 25–45. ISBN 9783319138756.
45. Barkoula, N.M.; Alcock, B.; Cabrera, N.O.; Peijs, T. Flame-Retardancy Properties of Intumescent Ammonium Poly(Phosphate) and Mineral Filler Magnesium Hydroxide in Combination with Graphene. *Polym. Polym. Compos.* **2008**, *16*, 101–113.
46. Baby, T.T.; Ramaprabhu, S. Investigation of Thermal and Electrical Conductivity of Graphene Based Nanofluids. *J. Appl. Phys.* **2010**, *108*, 124308. [CrossRef]
47. Warzoha, R.J.; Fleischer, A.S. Heat Flow at Nanoparticle Interfaces. *Nano Energy* **2014**, *6*, 137–158. [CrossRef]